

Direct Numerical Simulations of Type Ia Supernovae Flames I: The Landau-Darrieus Instability

J. B. Bell¹, M. S. Day¹, C. A. Rendleman¹, S. E. Woosley², M. Zingale²

ABSTRACT

Planar flames are intrinsically unstable in open domains due to the thermal expansion across the burning front—the Landau-Darrieus instability. This instability leads to wrinkling and growth of the flame surface, and corresponding acceleration of the flame, until it is stabilized by cusp formation. We look at the Landau-Darrieus instability for C/O thermonuclear flames at conditions relevant to the late stages of a Type Ia supernova explosion. Two-dimensional direct numerical simulations of both single-mode and multi-mode perturbations using a low Mach number hydrodynamics code are presented. We show the effect of the instability on the flame speed as a function of both the density and domain size, demonstrate the existence of the small scale cutoff to the growth of the instability, and look for the proposed breakdown of the non-linear stabilization at low densities. The effects of curvature on the flame as quantified through measurements of the growth rate and computation of the corresponding Markstein number. While accelerations of a few percent are observed, they are too small to have any direct outcome on the supernova explosion.

Subject headings: supernovae: general — white dwarfs — hydrodynamics — nuclear reactions, nucleosynthesis, abundances — conduction — methods: numerical

1. INTRODUCTION

A carbon/oxygen flame propagating outward from the center of a white dwarf is subjected to a number of instabilities that wrinkle and accelerate the flame. If the flame can

¹Center for Computational Science and Engineering, Lawrence Berkeley National Laboratory, Berkeley, CA 94720

²Dept. of Astronomy & Astrophysics, The University of California, Santa Cruz, Santa Cruz, CA 95064

accelerate to a significant fraction of the speed of sound, a deflagration alone can account for the explosion (see Hillebrandt & Niemeyer 2000 and references therein; Reinecke et al. 2002; Gamezo et al. 2003). One such instability, the Landau-Darrieus (LD) instability (Darrieus 1938; Landau 1944) affects a planar flame front, even in the absence of gravity, driven by the thermal expansion across the flame. The LD unstable flame will wrinkle, eventually forming cusps in the nonlinear regime that stabilize the flame. The growth rate for a LD unstable flame, including the effects of the finite thickness of the flame, l_f , is

$$\omega = kU_l \frac{\alpha}{\alpha + 1} \left[\sqrt{\alpha - \frac{1}{\alpha} + 1 + k l_f \text{Ma} (k l_f \text{Ma} + 2\alpha)} - 1 + k l_f \text{Ma} \right] \quad (1)$$

(Zeldovich et al. 1985), where $\alpha = \rho_{\text{fuel}}/\rho_{\text{ash}}$ is the density ratio across the flame, k is the wavenumber, U_l is the laminar flame speed, and Ma is the Markstein number. The Markstein number is a measure of the response of the flame speed, U , to curvature,

$$U = U_l \left(1 + \text{Ma} l_f \frac{\partial^2 y_f}{\partial x^2} \right) , \quad (2)$$

where y_f is the position of the flame interface and x is the transverse coordinate. We note that our sign convention for Ma is opposite that used in Zeldovich et al. (1985) (see Dursi et al. 2003 for a discussion of the Markstein number for astrophysical flames). This growth rate has been confirmed experimentally (Clanet & Searby 1998) for chemical flames. In this paper, we present two-dimensional direct numerical simulations (DNS) of the LD instability for low-density C/O flames in white dwarf interiors. We start by briefly reviewing previous LD simulations and results relevant for thermonuclear flames.

Sivashinsky (1977) and Michelson & Sivashinsky (1977) studied the non-linear regime of the LD instability analytically and numerically, using an integro-differential equation to describe the deformation of a discontinuous flame front. This was extended later by Gutman & Sivashinsky (1990), who concentrated on the regime where thermal conduction dominates over mass diffusion (this is the regime appropriate for astrophysical flames). They experiment with boundary conditions (both adiabatic and periodic) and discuss the influence of the domain size on the final cusp behavior. Their simulations show a multi-mode perturbation cusping, and slowly, the cusps merging until only a single one survives. In the widest domains, a superimposed cellular structure appears on the single remaining cusp. The mechanism behind this cellular instability does not, at this moment, seem to be well understood (although see Kupervasser et al. 1996). A similar approach, using a more general equation for the front, the Frankel equation, considering spherically expanding flames, was performed by Blinnikov & Sasorov (1996). They observe a fractal structure for the front through a range of spatial scales. The unstable flame exhibits cell-splitting, owing to the expanding

spherical geometry. Helenbrook & Law (1999) presented simulations that treat the fuel and ash states as incompressible, and link them with jump conditions across the discontinuous front. In contrast to other methods, feedback between the flame and fluid flow is included in this model. They found that the flow dominates the LD instability in setting the scale for the wrinkling. This has important consequences for the flame in Type Ia supernova (SNe Ia), as the medium will be turbulent, and some evidence suggests that a large-scale dipole flow is setup during the ignition phase of the explosion (Kuhlen et al. 2003). In the real star, it may be likely that the fluid motions swamp any effects of the LD instability. Furthermore, the LD instability will be competing with the Rayleigh-Taylor instability (Bell et al. 2003b).

Recently, front tracking methods treating a discontinuous flame coupled to full hydrodynamics have been used for both terrestrial (Qian et al. 1998) and astrophysical flames (Röpke et al. 2003) to investigate LD unstable flames. The work of Röpke et al. (2003) used a level set method coupled to fully compressible PPM (Colella & Woodward 1984) to follow a discontinuous flame front, using flame speeds from Timmes & Woosley (1992). In their highest resolution run, they report seeing a cellular structure distorting the single cusp, perhaps arising through the same process as described in Gutman & Sivashinsky (1990). Röpke et al. (2003) find the flame speed rising to $1.3\times$ the laminar speed.

The work described above all treat the flame as a discontinuous front—some model is required to describe the behavior of the flame on scales smaller than the grid resolution. The finite thickness of the flame is known to have some influence on the LD instability, such as setting the small scale cutoff for the growth, so simulations that resolve the thermal structure are important. Direct numerical simulations of the LD instability at various densities in the astrophysical context were performed by Niemeyer & Hillebrandt (1995), showing cusp formation, but it was unclear from their studies whether there was any acceleration over the laminar speed. Their lowest density flame ($5 \times 10^7 \text{ g cm}^{-3}$) showed significant growth beyond simple cusping, but it is likely that this was either numerical in origin, or due to the interaction of the transient perturbations left over from the initialization with the flame.

LD unstable flames in laminar flows are unlikely alone to lead to the accelerations required of the SNe Ia models. An interesting question is whether the non-linear stabilization can break down, whether through some property intrinsic to the flames or through external forces. Kerstein (1996) discusses one such mechanism, active turbulent combustion, involving the interaction of the LD unstable flame with turbulence. It has been proposed that this process could occur in Type Ia supernovae (Niemeyer & Woosley 1997), since large amounts of the thermonuclear energy released goes into the expansion of the star, and it is this thermal expansion that drives the LD instability. Niemeyer & Woosley (1997) argue that this feedback between the flame and its own turbulence could lead to large accelerations of

the flame, although, at present, this has not been demonstrated in numerical simulations.

We focus on DNS of the Landau-Darrieus instability at low densities ($\rho \sim 2 \times 10^7 \text{ g cm}^{-3} - 8 \times 10^7 \text{ g cm}^{-3}$) using a low Mach number numerical formulation, as described in Bell et al. (2003a). Here we are able to extend to lower densities than previous studies, and also, through the use of adaptive mesh refinement, use finer resolution and larger domains. For the present study, we restrict ourselves to two-dimensional calculations. These direct numerical simulations are truly parameter free (i.e., no laminar flame speed is input), and could serve to test/calibrate different methods of representing unresolved flames on stellar-sized domains. Corresponding DNS calculations of the Rayleigh-Taylor instability will be presented in a second paper (Bell et al. 2003b). Three-dimensional results will be presented in a future paper. Additionally, we do not look to seed the flow with turbulence in the present study, but rather choose to focus solely on the pure LD instability. We provide a brief description of the numerics and parameters used for the present simulations in §2. In §3, we discuss the results, and finally, in §4 we conclude.

2. NUMERICAL METHODS

The evolution was carried out using a low Mach number formulation of the Euler equations, as described in Bell et al. (2003a); Day & Bell (2000). The low Mach number formulation takes advantage of the fact that for slow moving flames, the pressure is constant across the flame front, to a high degree. Scaling the state variables and expanding them in powers of Mach number, keeping terms to $O(M^2)$ (Majda & Sethian 1985) yields a system of equations whose numerical stability condition is set by the fluid velocity alone, instead of the flow velocity plus sound speed. The pressure is decomposed into a dynamic and thermodynamic component, the ratio of which is of $O(M^2)$, with only the dynamic component appearing in the momentum equation. The equation of state is enforced by requiring the pressure to be constant along particle paths, resulting in an elliptic constraint on the velocity field, completing the system of equations. For the flames we consider in the present paper, $M < 10^{-4}$, so this approximation is valid. This allows for timesteps that are $O(1/M)$, larger than a corresponding compressible code.

The low Mach number equations are solved via a second-order, fractional-step advection/projection/reaction procedure. The advection step advances the fluid variables to the new timestep and finds a provisional velocity field that does not yet satisfy the elliptic constraint. The new velocities are found by projecting this velocity field onto the space that discretely satisfies the elliptic constraint. Reactions are included via Strang-splitting. We refer the reader to Bell et al. (2003a) for the full details of the numerical method, as it is

unchanged for the present study. Laminar astrophysical flames computed with this code were compared to the benchmark calculations presented in Dursi et al. (2003), and found to be in good agreement.

The calculations we present here differ from the fully compressible PPM (Colella & Woodward 1984) method used in Niemeyer & Hillebrandt (1995) in several fundamental ways. First, the low Mach number formulation yields a timestep constraint that depends only on the fluid velocity, not the fluid velocity and sound speed as in the compressible case. This means that we can take much larger timesteps, which for very slow moving flames, greatly reduces the accumulation of error. Additionally, the advection algorithm we employ is not dimensionally split, reducing the influence of the grid on the flame. Finally, the two dimensional domain is initialized by mapping a steady state flame in a perturbed fashion onto the grid, rather than perturbing an interface between fuel and ash and waiting for the flame to develop. This significantly reduces the transients and leaves the flow ahead of the flame unperturbed.

An equation of state with degenerate/relativistic electrons and positrons, ideal gas ions, and Boltzmann radiation was used, as described in Timmes & Swesty (2000). The thermal conductivity is described in Timmes (2000). A single reaction, $^{12}\text{C}(^{12}\text{C},\gamma)^{24}\text{Mg}$, is followed, using the unscreened rate from Caughlan & Fowler (1988). This accounts for the bulk of the energy generation in a C/O flame. Furthermore, at the densities we are considering, burning is expected to terminate at intermediate mass elements, so stopping at ^{24}Mg is reasonable. For this simple burning rate, we ignore the effects of the oxygen on the energy generation—it is only advected passively here. The temperatures reached behind the flame at these densities are $\sim 4 \times 10^9$ K. At these temperatures, oxygen burning is several orders of magnitude slower than carbon, and we would not expect any effects from it on the timescales that we follow the flames. The properties of the flames we consider here are listed in Table 1. We will consider the 4×10^7 g cm $^{-3}$ flame to be our reference flame, upon which we will explore the effects of resolution and domain size.

Motivated by results indicating that multi-mode perturbations eventually merge into a single dominant cusp (see for example Gutman & Sivashinsky 1990; Bell et al. 2003a), we concentrate mainly on single mode perturbations. In all cases, the flame is initialized on the grid by mapping a steady-state one-dimensional laminar flame across the grid, shifting it vertically according to the perturbation. The boundary conditions in all cases are periodic transverse to the flame propagation direction, inflow ahead of the flame, and outflow behind the flame. The flame is oriented such that it is propagating downward in our domain. The inflow conditions correspond to the fuel conditions, with the inflow velocity chosen to match the laminar flame velocity. Thus, a flame moving at the laminar speed will remain stationary

in the computational domain. Any acceleration resulting from the flame instability will lead to motion across the grid. The resolution used is chosen to put about 5–10 zones inside the thermal width, l_f , calculated as

$$l_f = \frac{T_{\text{ash}} - T_{\text{fuel}}}{\max(\nabla T)} , \quad (3)$$

where T_{ash} and T_{fuel} are the ash and fuel temperatures respectively. We note that this flame width measure is ~ 2 times narrower than that used in Timmes & Woosley (1992) (see also Dursi et al. 2003). In §3, we look at the sensitivity of the results to the resolution.

3. RESULTS

3.1. Multi-mode perturbations

As a motivation for the single mode studies, we look at a single case of a multi-mode perturbation of a $4 \times 10^7 \text{ g cm}^{-3}$ flame in a 20.48 cm wide domain. The flame front was perturbed by shifting the zero point of the initial steady state flame by a sinusoid, with 30 different frequencies, whose phases and amplitudes were chosen randomly. The maximum amplitude of the perturbation is one flame thickness. Figure 1 shows the y -velocity at several instances in time. We see that immediately, the higher frequency perturbations are washed out, and only the long wavelength modes slowly begin to grow. Several cusps begin to form, but quickly merge, leaving two dominant cusps behind. These remaining cusps gradually move toward each other (through the periodic boundary), eventually merging, leaving a single dominant cusp behind. The timescale for the cusps to merge is long, ~ 2 ms, so we show only one case here. Bell et al. (2003a) shows another example, for a pure carbon flame at a higher density, following the evolution for several cusp mergers.

The flame speed can be measured by computing the carbon destruction rate on the grid, taking into account the flow of material through the boundaries:

$$F(t) = -\frac{\int_0^t \int_{\Omega} \rho \dot{\omega}_c d\mathbf{x} dt}{W(\rho X_c)^{\text{in}}} \quad (4)$$

where Ω is the spatial domain of the burning region, W is the width of inflow face, $(\rho X_c)^{\text{in}}$ is the inflow carbon mass fraction, and $\rho \dot{\omega}_c$ is the rate of consumption of carbon due to nuclear burning. The rate of change of this quantity in a time interval $[T_1, T_2]$ is a measure of effective flame velocity:

$$V_{\text{eff}} = \frac{\int_{\Omega} (\rho X_c)|_{T_1}^{T_2} d\mathbf{x}}{(T_2 - T_1)W(\rho X_c)^{\text{in}}} - u^{\text{in}} \quad (5)$$

Figure 2 shows the flame speed as a function of time for the multimode calculation. After an initial, relatively constant velocity period, in which the initial perturbations die out, the flame begins to accelerate rapidly. The velocity peaks shortly after the leftmost two initial cusps merge, leaving behind two well defined cusps. A second peak occurs at the merging of these two cusps.

The merging of multiple cusps into a single dominant one has been observed in other planar flame simulations (see for example Gutman & Sivashinsky 1990; Helenbrook & Law 1999), and it seems to be a general feature of the LD instability, with the exception of spherically expanding flames (Blinnikov & Sasorov 1996). We note however that we see no evidence for a superposed cellular structure on the remaining cusp, but this may be due to domain size restrictions (Gutman & Sivashinsky 1990). The final cusp that emerges is robust and shows no signs of breaking down.

3.2. Single-mode perturbations

The main focus of the present study is to look at the acceleration that a flame undergoing the LD instability will experience, in the absence of any external forcing. In particular, we wish to determine whether there is any breakdown of the cusp configuration. Since the general consensus is that multimode perturbations in planar domains tend to merge into a single, well defined cusp, we can seed a single mode to study the behavior of this steady state configuration.

Table 2 list the parameters used for the single-mode calculations. In addition to a run of densities, we considered the effect of the box width and resolution on the instability for one choice of density ($4 \times 10^7 \text{ g cm}^{-3}$). The reference calculation at this density is a 10.24 cm wide \times 20.48 cm high domain, with a resolution of 6 points in the flame width, l_f . Numerical experiments have shown that this resolution is enough to accurately follow the flame front (see Bell et al. 2003a). The critical wavelength for the growth of 1/2 carbon, 1/2 oxygen astrophysical flames over a range of densities was computed in Dursi et al. (2003), who, when converted to the flame thickness definition used here, found ~ 80 flame thicknesses to be the small scale cutoff. If this result holds for the densities we consider here, then for domains narrower than 80 flame widths, we do not expect the LD instability to be able to grow. We note that our reference domain width is ~ 174 flame widths wide, which should be well above the small scale cutoff for the LD growth. We will find this small scale cutoff directly by varying our domain width, computing the Markstein number, and finding the zeros of the LD dispersion relation, Equation (1). A single sine wave perturbation was used as an offset when mapping the steady state laminar flame profile onto the domain.

Figure 3 shows the x - and y - velocities for the reference $4 \times 10^7 \text{ g cm}^{-3}$ LD flame once the cusp has become well defined. After this point, the flame front retains this shape. As with the cusps in the multimode simulation, we see that the vertical velocity peaks strongly right behind the cusp, and then drops below the ambient post flame velocity as one moves further away from the flame front. One thing to note from these velocity figures is how smooth the flow is ahead of and behind the flame. There is virtually no noise to disturb the pure LD instability. Figure 4 illustrates this by showing two slices of the y -velocity—through the center of the cusp and the center of the trough—when the cusp is at its maximum. This behavior is a natural consequence of the local curvature and its effect on the velocity streamlines. The change in the peak carbon destruction rate as a function of curvature is shown in Figure 5. The curvature was computed by finding the position of the front and taking the second derivative. We see that the larger the magnitude of the curvature, the greater the carbon destruction rate. At zero curvature, the carbon destruction rate is the laminar value. The scatter in the plot reflects the difficulty in defining the curvature for a discretely defined interface.

Figure 6 shows the flame speed as a function of time for the $4 \times 10^7 \text{ g cm}^{-3}$ C/O flame in several different sized domains (2.56 cm, 5.12 cm, 10.24 cm, and 20.48 cm). The flame speed was computed by looking at the carbon consumption rate as in Equation (5). As the box width was varied, we choose to make $\delta y/W$ constant, where δy is the perturbation amplitude, and W is the box width. All other parameters (i.e., box height, boundary conditions, etc.) were held constant across the different simulations. The velocity of the flame for the two widest domains increases quickly and reaches a peak, where it levels off, at a value about 1.6% higher than the laminar speed. The slight decrease in the flame speed at late times for the 10.24 cm run is likely a result of the finite vertical extent of the domain. The 5.12 cm domain run evolves much more slowly. This domain is ~ 87 flame widths wide, right at the small scale cutoff for the LD instability. We believe that the slow growth that we see is a manifestation of this cutoff. The narrowest domain (2.56 cm) does not grow at all. It is not known what accounts for the small difference in the asymptotic flame speeds for the two widest domains.

We can compare the time it takes for the flame speed to saturate to the theoretical prediction of the LD growth rate, Equation (1). The amplitude of the cusp is computed by laterally averaging the carbon mass fraction, and finding the positions where it exceeds 0.05 and 0.45. Figure 7 shows the height of the cusp as a function of time for the 10.24 cm and 20.48 cm wide runs. Looking at these plots, there is clearly a regime of linear growth followed by a transition to the nonlinear regime where the cusping halts the growth, and the amplitude reaches a steady state value. The solid line is a fit to

$$y = Ae^{\omega t} , \tag{6}$$

for the interval of 1×10^{-4} to 4×10^{-4} s (the linear regime), which gives $\omega = 3968$ and 3046 respectively—the narrower domain grows faster. We ignored the very first part of the growth to avoid any transients. If we were to ignore the effects of curvature and the flame thickness (i.e., set $\text{Ma} = 0$ in Equation [1]), we would get predictions of $\omega = 8200$ and 4100 for these domains. Thus, the finite thickness of the flame slows down the growth of the LD instability, demonstrating the effects of the curvature on the flame speed.

The finite thickness imposes a small scale cutoff to the LD growth, which we can now compute. Using the flame data from Table 1, we can solve for the Markstein number, and find $\text{Ma} = -2.45$ for both of these domain widths. A negative value is to be expected, as it indicates that a positively curved flame burns more slowly, which is expected for our flames where thermal diffusion dominates mass diffusion (Dursi et al. 2003). With this value of the Markstein number, we can plot the growth rate as a function of wavenumber, Figure 8. We see that the LD stops growing for dimensionless wavenumbers larger than 0.07, or domain widths smaller than 5.28 cm. This is consistent with behavior of the 2.56 cm and 5.12 cm runs we showed above. For this reason, we do not perform fits to these narrowest domain runs. The maximum growth should be seen for dimensionless wavenumbers of 0.035, or a domain with of 10.6 cm. Looking back at Figure 6, we see that the 10.24 cm run (our closest domain width to this maximum) reached the peak velocity quickest and had the largest growth rate (as determined by the fits to the cusp amplitude growth), consistent with the dispersion relation. This also explains why the multimode perturbation presented above went through an intermediate phase consisting of two cusps. There, the domain was 20.48 cm wide, and perturbations were made on many length scales. The dispersion relation predicts that the 10.6 cm perturbations will grow fastest, overwhelming any smaller perturbations. This means that the mode that we seeded that put two wavelengths in the box would grow the fastest, resulting in the intermediate, moderately long lived state with two cusps.

Figure 9 shows the flame speed vs. time for the 10.24 cm wide, 4×10^7 g cm $^{-3}$ run at three different resolutions. The flame speed is normalized to the laminar speed at that resolution to account for the small resolution dependence on this speed. Table 3 lists the laminar flame speeds for the different resolutions. At the highest resolutions, the laminar flame speeds differ by 0.13%, and the normalized velocity vs. time curves lie on top of one another, demonstrating convergence. The coarsest resolution laminar flame speed differs by 1.1%, and the evolution with time is clearly not converged. All the simulations presented in this paper are performed at this middle resolution or higher. This resolution agrees with that found in the corresponding resolution study in Bell et al. (2003a).

Figures 10 and 11 show the flame speed as a function of time for the 2×10^7 g cm $^{-3}$ and 8×10^7 g cm $^{-3}$ runs respectively. The evolution at these densities proceeded in much the same

way as the $4 \times 10^7 \text{ g cm}^{-3}$ run shown in Figure 3, so we do not show the velocity fields. Only one domain width was used for these calculations, with the size picked close to the wavelength that maximizes the growth rate. The change in density (and expansion parameter across the flame) changes the speedup we get. The $2 \times 10^7 \text{ g cm}^{-3}$ flame accelerates by 2.4% and the $8 \times 10^7 \text{ g cm}^{-3}$ flame by 1.1%. Together with the results for the $4 \times 10^7 \text{ g cm}^{-3}$ flame, we see that the acceleration is larger for the lower density/larger expansion ratio flames. We can compute the Markstein numbers for these flames in the same manner as above and find -3.42 and -2.02 for the $2 \times 10^7 \text{ g cm}^{-3}$ and $8 \times 10^7 \text{ g cm}^{-3}$ flames respectively (see Figures 12 and 13). Again, the fit of an exponential to the linear portion of the growth is excellent. The dispersion relations for these flames are also plotted in Figure 8. To fit them all on the same plot, the curves are scaled by the flame speed and width. The magnitude of the Markstein number increases with decreasing density and increasing expansion parameter. This is not unexpected, and confirms the trend seen in Dursi et al. (2003) for similar flames. This suggests that a lower density flame is harder to bend.

As a final measure of the effects of curvature on the flame speed, we can compare the growth in the flame surface area to the growth in flame speed. In the simplest model, these two are directly related in a purely geometrical fashion, and the flame speed would be simply

$$v(t) = v_0 \frac{A(t)}{A_0} . \quad (7)$$

We can measure the length of the flame surface by counting the number of zone edges where the carbon mass fraction passes through 0.25. This measure agrees well with computing the length of a contour as computed with the commercial IDL package, after normalization. Since the flame surface is always sharp, this is a well-defined procedure. Figure 14 shows the normalized flame length as a function of time for the three different densities (the 10.24 cm reference run was used for the $4 \times 10^7 \text{ g cm}^{-3}$ case). In all these cases, the increase in the flame length is several times larger than the increase in the flame speed, showing a strong deviation from the linear scaling of Equation (7)—for example, the $4 \times 10^7 \text{ g cm}^{-3}$ flame increases in speed by about 1.6%, but the area increase is 12%. This deviation is due to the effects of the localized curvature. We note that this deviation is larger in magnitude than that found in the compressible, flame-model calculations of Röpke et al. (2003).

4. CONCLUSIONS

We presented direct numerical simulations of the Landau-Darrieus instability at low densities in conditions relevant for Type Ia supernova explosions. We employed a low Mach number hydrodynamics method—new in the application to astrophysics—to advance the

flows and enable us to follow the development of the LD instability from the linear regime through the nonlinear regime. Resolving the flame ensures that we account for the full coupling between the flame and the flow and the effects of curvature. The consistency of our results with the theoretical predictions validate this approximation for astrophysical flames. Fully compressible versions of the same simulations would not be possible, or prohibitively expensive and error prone.

Acceleration of the flame was seen, due to the increase of flame surface, until the nonlinear cusp formation sets in, at which point the velocity stabilized a few percent higher than the laminar speed. The maximum increase in flame speed observed was $\sim 2\%$ —this is in contrast to the results presented in Röpke et al. (2003), where accelerations of $\sim 30\%$ were observed. There are several possible reasons to explain these differences. Most of the numerical results for the LD instability treat the flame as infinitely thin. Here we’ve included the effects of the finite thickness of the flame, and therefore, implicitly included curvature effects. At the densities we consider, the burning is expected to terminate at the intermediate mass elements, so we burn to magnesium whereas they burn to nickel. Furthermore we use half carbon/half oxygen fuel instead of pure carbon. This will affect the expansion factor across the flame. Finally, fully understanding the role of the numerics requires a detailed comparison of the different methods, using the same input physics, and could potentially be a research project in the future.

The speedup increases with decreasing density (or increasing expansion parameter), as expected. With time, it seems as if the velocities asymptote to the same value, for a given density. When a multimode perturbation is considered, it is observed that the cusps eventually merge into a single cusp.

We were able to perform fits of the growth of the cusp amplitude with time to compute the growth rates. Using the theoretical prediction (Equation [1]), we were able to compute the Markstein number for these flames, finding values < -2.0 , and growing in magnitude with decreasing density. These values and the trend with density are consistent with the results of Dursi et al. (2003). For the $4 \times 10^7 \text{ g cm}^{-3}$ density run, the large number of domain widths allowed us to compare to the predictions of the fastest growing mode and small scale cutoff from the theoretical dispersion relation, and we found strong agreement. Furthermore, this demonstration of the small scale cutoff and the deviation from the infinitely thin flame ($\text{Ma} = 0$) estimates of the growth rate, as well as the difference in the growth of the flame speed and area emphasize the importance of curvature in small-scale flame dynamics. As we zoom out from these fully resolved flames, several steps will be needed at intermediate scales between the fully resolved flame, where curvature effects appear important, and the full star, with validation of the flame model on each scale through direct comparison to the

immediately smaller scale simulations. The present direct numerical simulations provide the anchor for this subgrid model validation. These curvature effects will be explored more fully in paper II, focusing on the reactive Rayleigh-Taylor instability.

We saw no breakdown of the nonlinear stabilization mechanism as hinted to in the calculations presented by Niemeyer & Hillebrandt (1995). Furthermore, none of the flames we studied showed a superposed cellular structure, although, there is some evidence (Gutman & Sivashinsky 1990) that this phenomena is present only on very large scales, and Blinnikov & Sasorov (1996) admit that it may actually be seeded by numerical noise. The widest domain that we were able to simulate was ~ 350 flame widths. Helenbrook & Law (1999) only saw this instability when they increased their domain size to 20 times the wavelength where the LD growth rate is the maximum. This would translate into a domain size of 230 cm for the $4 \times 10^7 \text{ g cm}^{-3}$ flame, which would require a 23,000 zone wide simulation if we are to resolve the flame. The growth rate for a domain that wide would be very small, requiring a much longer simulation. This is very expensive, and furthermore, it is not known if this factor of 20 is universal. We are not aware of any resolved calculations of the LD instability that have shown this secondary instability.

We note that all of our calculations considered planar geometries only. On the scales where the spherical geometry of the star is likely to make a difference, the flame will be disturbed by the larger scale motions in the star, other instabilities as well (notably the Rayleigh-Taylor instability, presented in Bell et al. 2003b) and subjected to the interaction with flame-generated turbulence. All of these processes will dominate the pure LD instability, considered in the present paper.

The authors thank L. J. Dursi for useful comments on the manuscript and F. X. Timmes for making his equation of state and conductivity routines available on-line. Support for this work was provided by the DOE grant number DE-FC02-01ER41176 to the Supernova Science Center/UCSC and the Applied Mathematics Program of the DOE Office of Mathematics, Information, and Computational Sciences under the U.S. Department of Energy under contract No. DE-AC03-76SF00098. The calculations presented here were performed on the IBM Power4 (cheetah) at ORNL, sponsored by the Mathematical, Information, and Computational Sciences Division; Office of Advanced Scientific Computing Research; U.S. DOE, under Contract No. DE-AC05-00OR22725 with UT-Battelle, LLC and the UCSC UpsAnd cluster supported by an NSF MRI grant AST-0079757.

REFERENCES

- Bell, J. B., Day, M. S., Rendleman, C. A., Woosley, S. E., & Zingale, M. A. 2003a, *Journal of Computational Physics*, to appear, preprint available at: http://seesar.lbl.gov/CCSE/Publications/car/LMN_nucl_flames.pdf
- . 2003b, *ApJ*, in preparation
- Blinnikov, S. I., & Sasorov, P. V. 1996, *Phys. Rev. E*, 53, 4827
- Caughlan, G. R., & Fowler, W. A. 1988, *Atomic Data and Nuclear Data Tables*, 40, 283, see also <http://www.phy.ornl.gov/astrophysics/data/cf88/index.html>
- Clanet, C., & Searby, G. 1998, *Physical Review Letters*, 80, 3867
- Colella, P., & Woodward, P. R. 1984, *J. Comp. Phys.*, 54, 174
- Darrieus, G. 1938, unpublished work presented at La Technique Moderne
- Day, M. S., & Bell, J. B. 2000, *Combust. Theory Modelling*, 4, 535
- Dursi, L. J., Zingale, M., Calder, A. C., Fryxell, B., Timmes, F. X., Vladimirova, N., Rosner, R., Caceres, A., Lamb, D. Q., Olson, K., Ricker, P. M., Riley, K., Siegel, A., & Truran, J. W. 2003, *ApJ*, 595, 955
- Gamezo, V. N., Khokhlov, A. M., Oran, E. S., Chtchelkanova, A. Y., & Rosenberg, R. O. 2003, *Science*, 299, 77
- Gutman, S., & Sivashinsky, G. I. 1990, *Physica D*, 43, 129
- Helenbrook, B. T., & Law, C. K. 1999, *Comb. Flame*, 117, 155
- Hillebrandt, W., & Niemeyer, J. C. 2000, *Annu. Rev. Astron. Astrophys.*, 38, 191
- Kerstein, A. R. 1996, *Combustion Sci. Technol.*, 118, 189
- Kuhlen, M., Woosley, S. E., & Glatzmaier, G. 2003, *Astrophysical Journal*, in preparation
- Kupervasser, O., Olami, Z., & Procaccia, I. 1996, *Physical Review Letters*, 76, 146
- Landau, L. D. 1944, *Acta Physicochimica, USSR*, 19, 77, reprinted in P. Pelcé, *Dynamics of Curved Fronts*, Academic Press, Berkeley, CA, 1988
- Majda, A., & Sethian, J. A. 1985, *Combust. Sci. Technol.*, 42, 185

- Michelson, D. M., & Sivashinsky, G. I. 1977, *Acta Astronautica*, 4, 1207
- Niemeyer, J. C., & Hillebrandt, W. 1995, *ApJ*, 452, 779
- Niemeyer, J. C., & Woosley, S. E. 1997, *ApJ*, 475, 740
- Qian, J., Tryggvason, G., & Law, C. K. 1998, *JCP*, 144, 52
- Röpke, F. K., Niemeyer, J. C., & Hillebrandt, W. 2003, *ApJ*, 588, 952
- Reinecke, M., Hillebrandt, W., & Niemeyer, J. C. 2002, *A&A*, 391, 1167
- Sivashinsky, G. I. 1977, *Acta Astronautica*, 4, 1177
- Timmes, F. X. 2000, *ApJ*, 528, 913
- Timmes, F. X., & Swesty, F. D. 2000, *ApJS*, 126, 501
- Timmes, F. X., & Woosley, S. E. 1992, *ApJ*, 396, 649
- Zeldovich, Y. B., Barenblatt, G. I., Librovich, V. B., & Markhiladze, G. M. 1985, *The Mathematical Theory of Combustion and Explosions* (New York: Consultants Bureau)

Table 1: Flame properties for 0.5 $^{12}\text{C}/0.5$ ^{16}O flames.

ρ (g cm $^{-3}$)	α^a	v_{laminar} (cm s $^{-1}$)	l_f (cm)
2×10^7	1.69	1.50×10^4	0.26
4×10^7	1.52	6.08×10^4	0.059
8×10^7	1.39	2.04×10^5	0.011

$^a\alpha = \rho_{\text{fuel}}/\rho_{\text{ash}}$

Table 2: Parameters for single mode Landau-Darrieus simulations.

ρ (g cm $^{-3}$)	description	$W \times H$ (cm)	fine grid	W/l_f	$l_f/\Delta x$
2×10^7	...	51.20×102.4	1536×3072	199.2	7.7
4×10^7	very narrow	2.56×20.48	256×2048	43.4	5.9
	narrow	5.12×20.48	512×2048	86.8	5.9
	regular	10.24×20.48	1024×2048	173.6	5.9
	wide	20.48×20.48	2048×2048	347.2	5.9
	low-resolution	10.24×20.48	512×2048	173.6	3.0
	high-resolution	10.24×20.48	2048×4096	173.6	11.8
8×10^7	...	2.56×3.84	2048×3072	232.7	8.8

Table 3: 4×10^7 g cm $^{-3}$ laminar flame speed vs. resolution

$l_f/\Delta x$	v_{laminar} (cm s $^{-1}$)
3.0	6.013×10^4
5.9	6.074×10^4
11.8	6.082×10^4

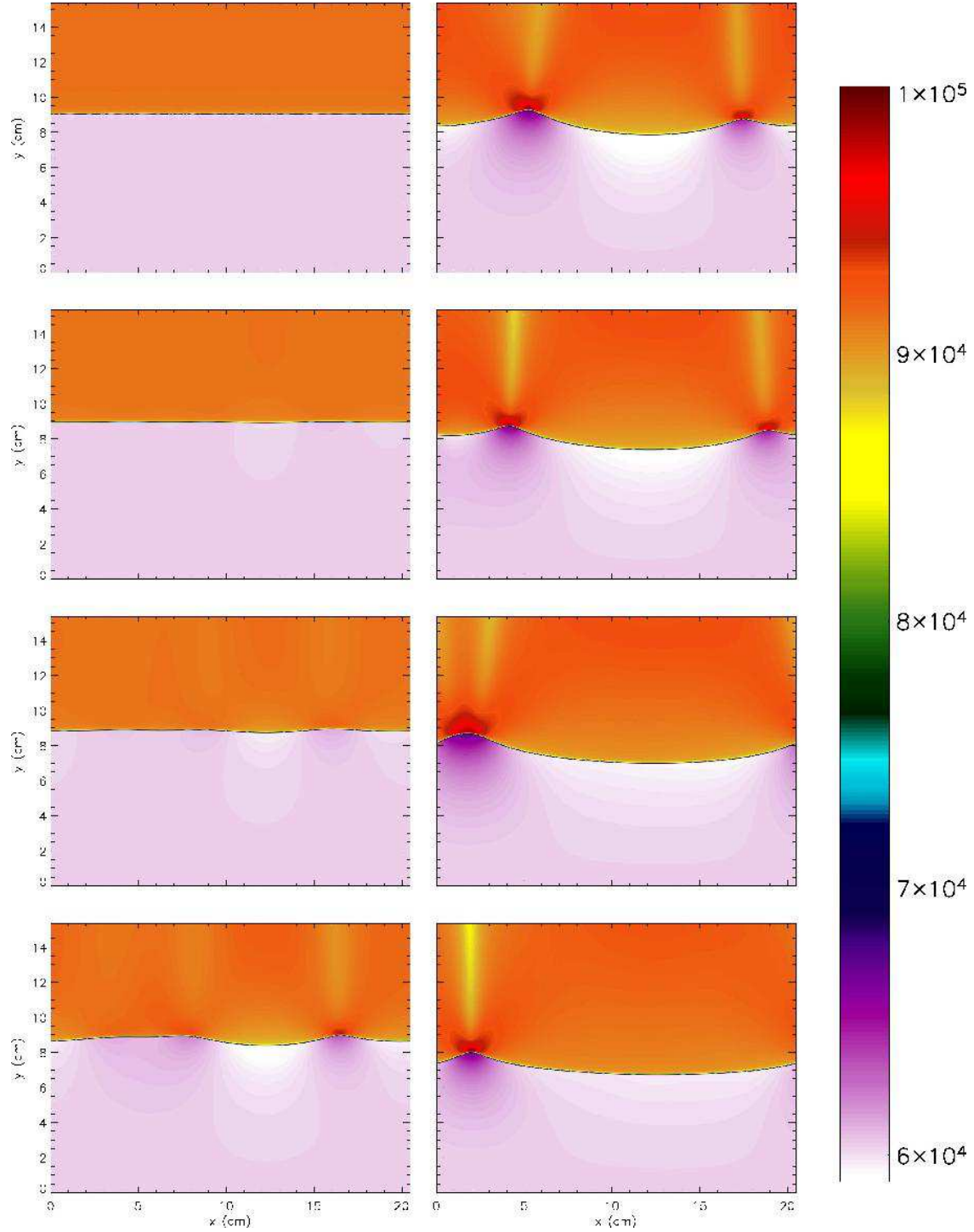


Fig. 1.— y -velocity for a $4 \times 10^7 \text{ g cm}^{-3}$ C/O flame undergoing a Landau-Darrieus instability. In this simulation, 30 different modes were perturbed. Each pane is $3 \times 10^{-4} \text{ s}$ apart, spanning 0 s to $2.1 \times 10^{-3} \text{ s}$. The initial perturbation rapidly evolves to only a few growing modes, and quickly, two cusps form that dominate the flow. Slowly, these two cusps move toward each other and merge through the periodic boundary, leaving a single, well-defined cusp behind.

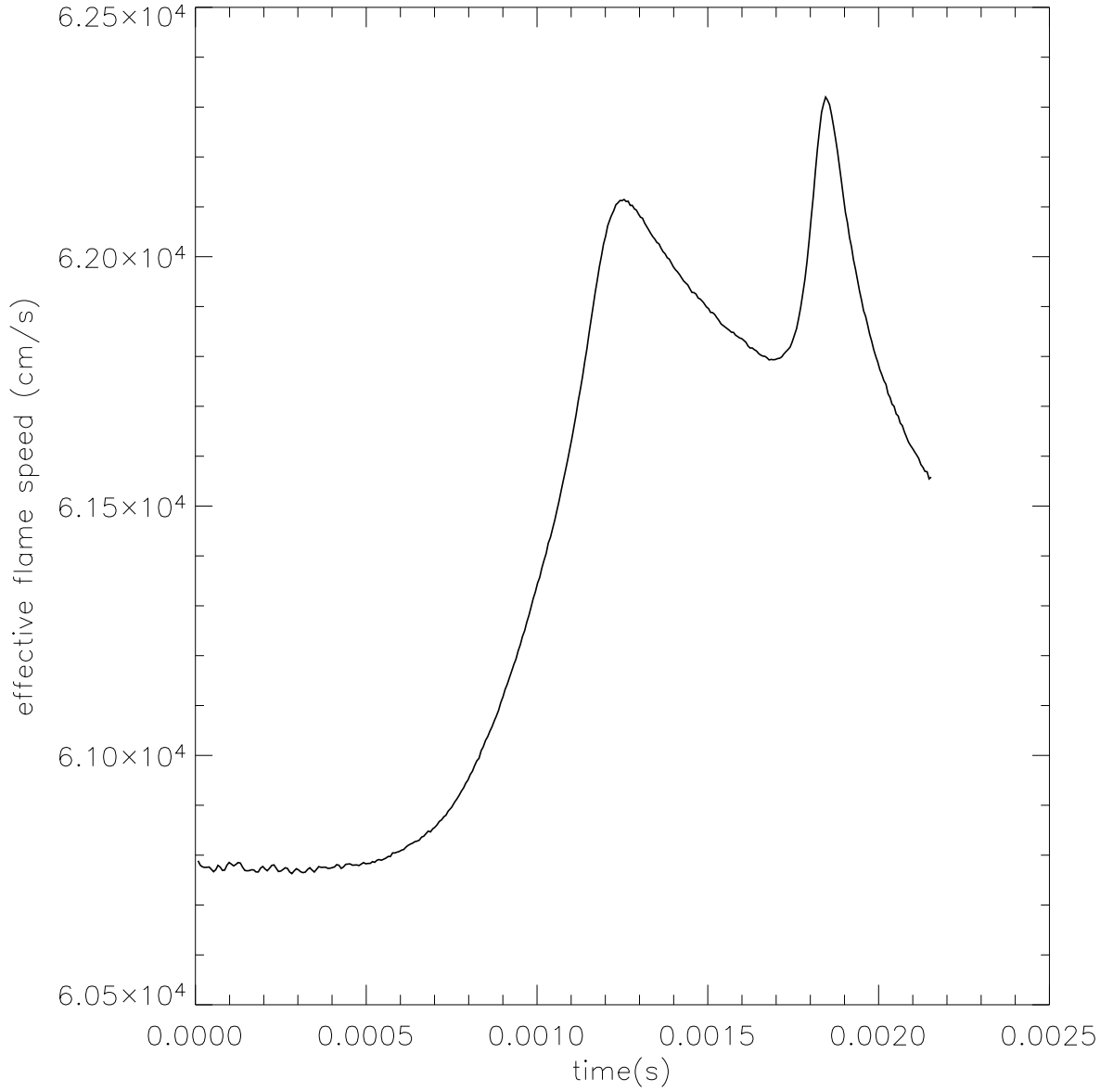


Fig. 2.— Flame speed as a function of time for the $4 \times 10^7 \text{ g cm}^{-3}$ C/O multimode Landau-Darrieus instability, shown in Figure 1.

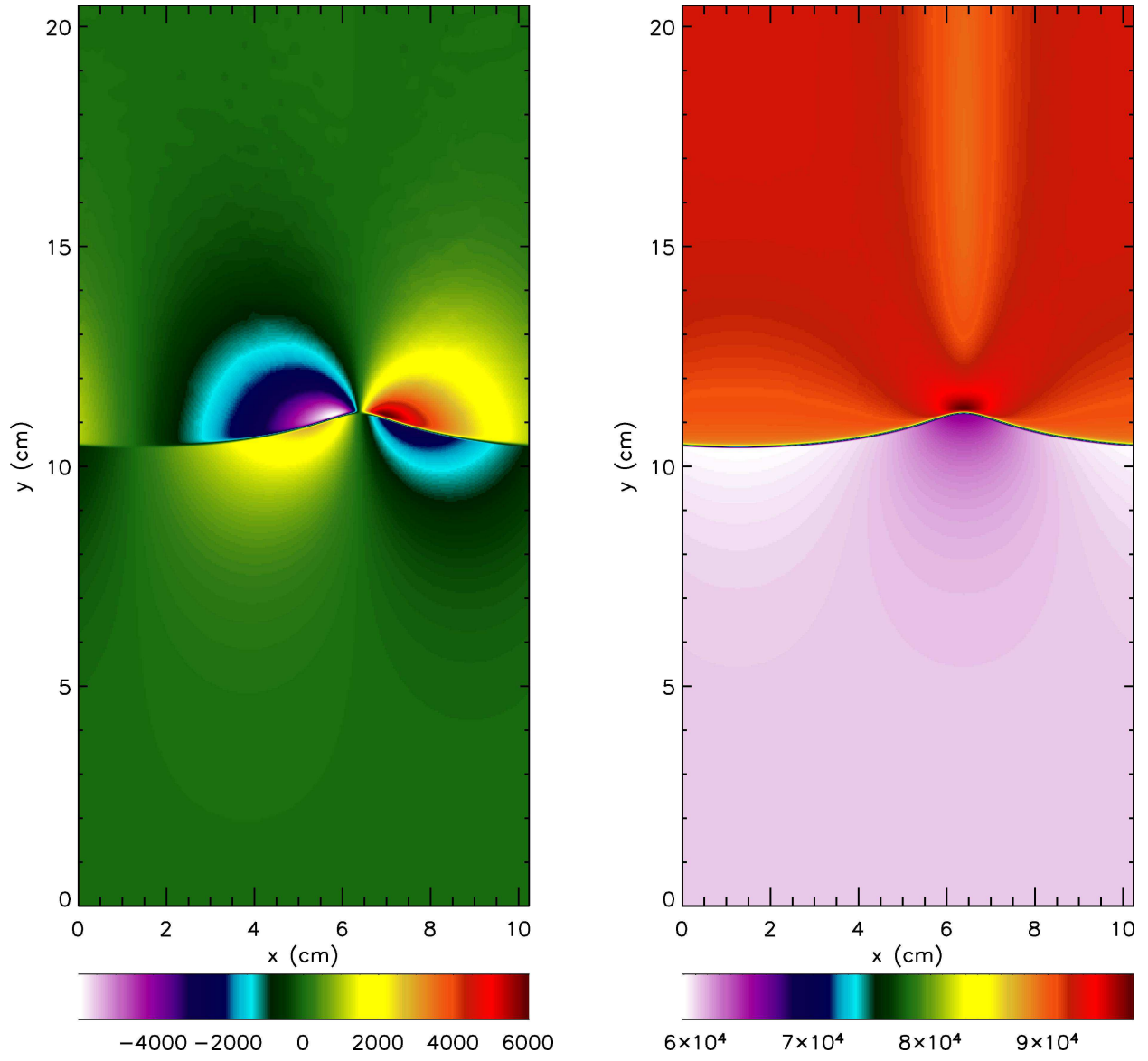


Fig. 3.— x -velocity (left) and y -velocity (right) for the high-resolution, 10.24 cm wide $4 \times 10^7 \text{ g cm}^{-3}$ flame perturbed with a single mode after $5 \times 10^{-4} \text{ s}$.

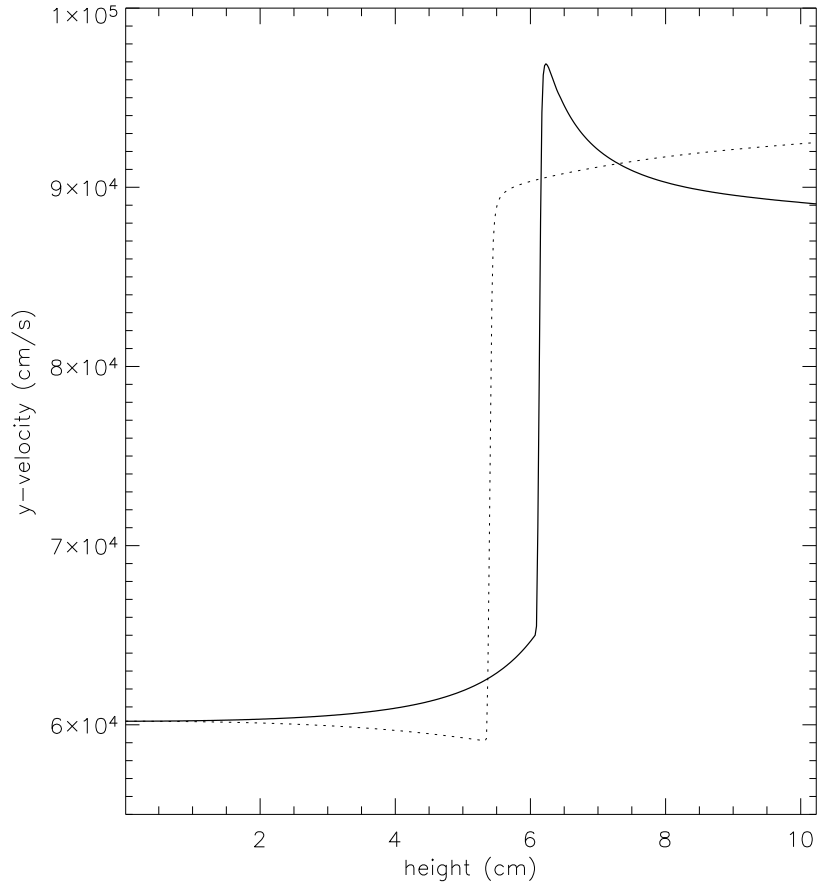


Fig. 4.— y -velocity for the 10.24 cm wide, $4 \times 10^7 \text{ g cm}^{-3}$ flame perturbed when the flame velocity is maximum ($6.29 \times 10^{-4} \text{ s}$) at the peak of the cusp (solid line) and the middle of the trough (dotted line). This demonstrates that the curvature leads to a change in the flame speed at different points along the flame front.

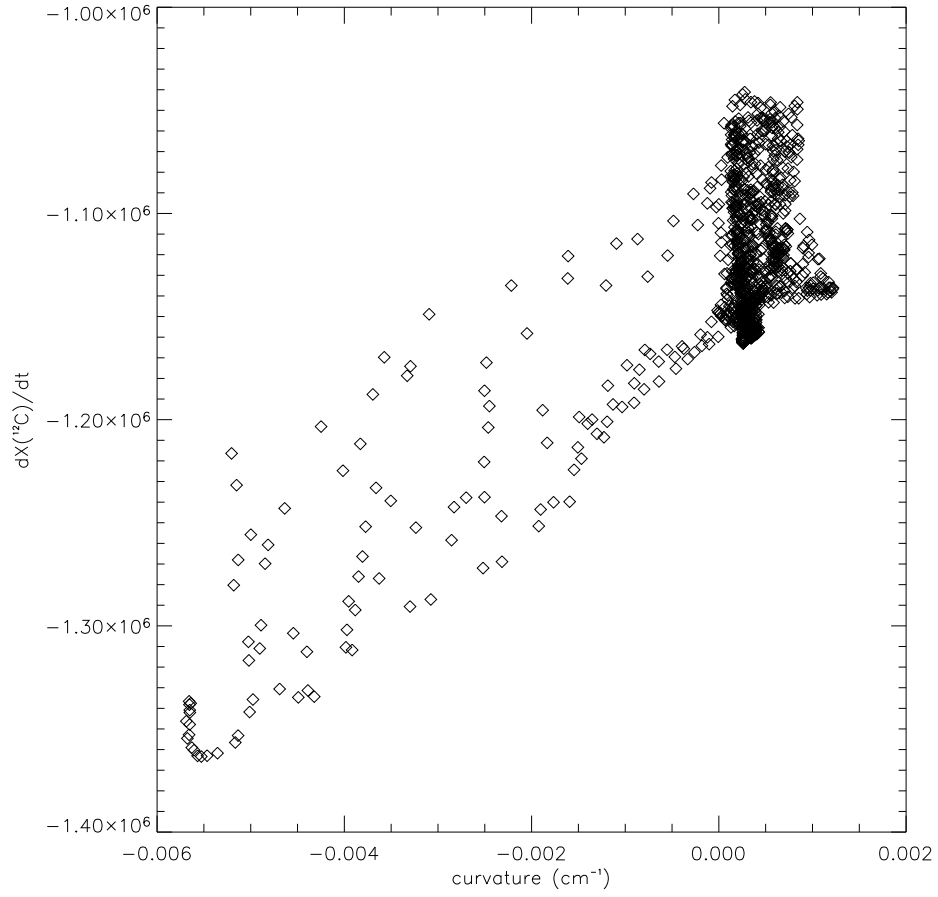


Fig. 5.— Carbon destruction rate vs. curvature ($d^2y_{\text{interface}}/dx^2$) for the 10.24 cm wide, $4 \times 10^7 \text{ g cm}^{-3}$ flame. When there is zero curvature, the carbon destruction rate is the laminar value.

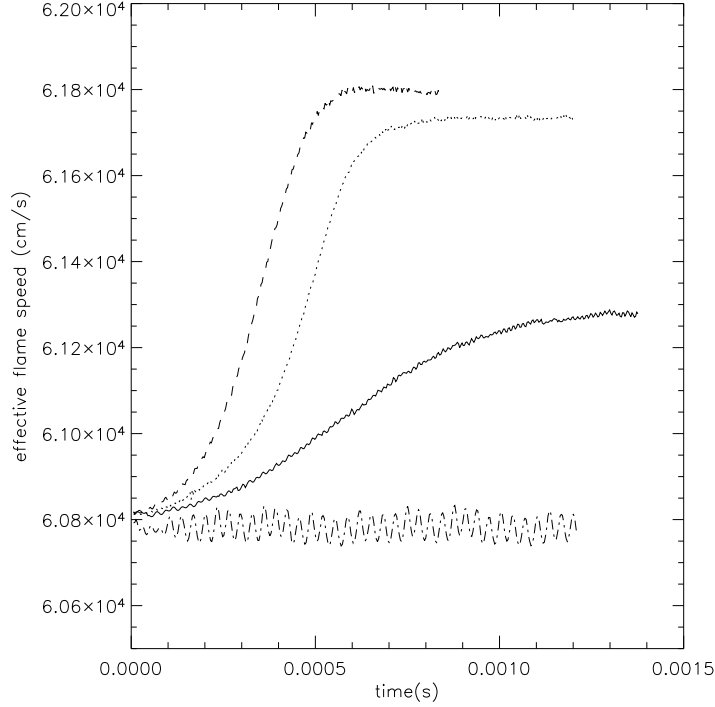


Fig. 6.— Flame speed vs. time for the $4 \times 10^7 \text{ g cm}^{-3}$ LD unstable flame in a 20.48 cm domain (dot) 10.24 cm domain (dash), 5.12 cm domain (solid), and 2.56 cm domain (dot-dash). The slow growth of the 5.12 cm wide run reflects the influence of this width being near the small scale cutoff for the growth of the LD instability. The 2.56 cm run shows no signs of growing, as expected, since that domain width is well below the small scale cutoff. The 10.24 cm wide domain rises the fastest, as expected, since this is closest to the maximum $\omega(k)$ of Equation [1] for this flame.

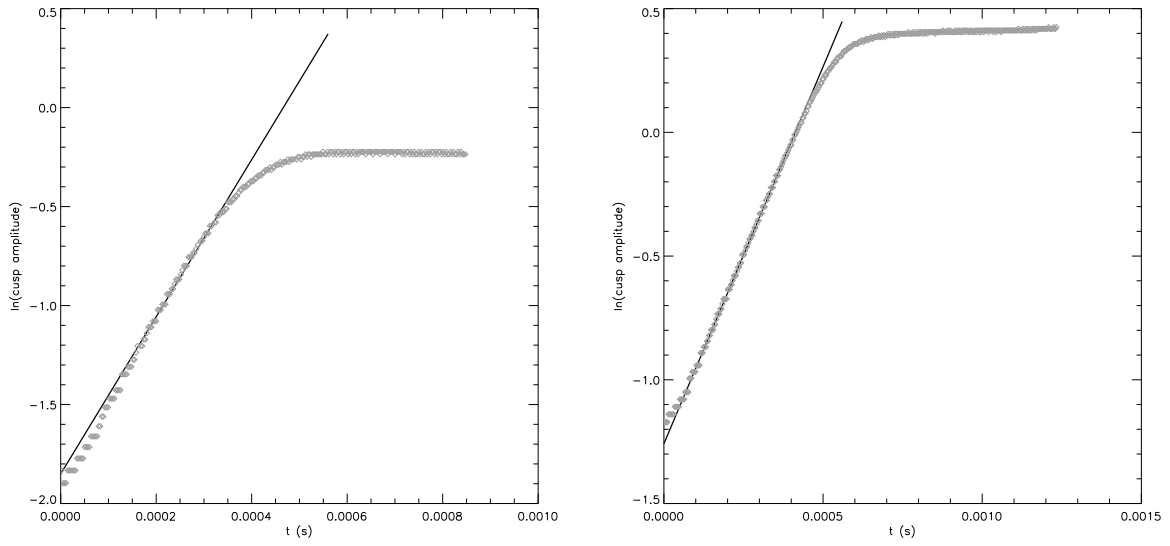


Fig. 7.— Height of the cusp (natural log scale) as a function of time (symbols) and a fit on an exponential to the linear part (solid line) for the 10.24 cm wide domain (left) and the 20.48 cm wide domain.

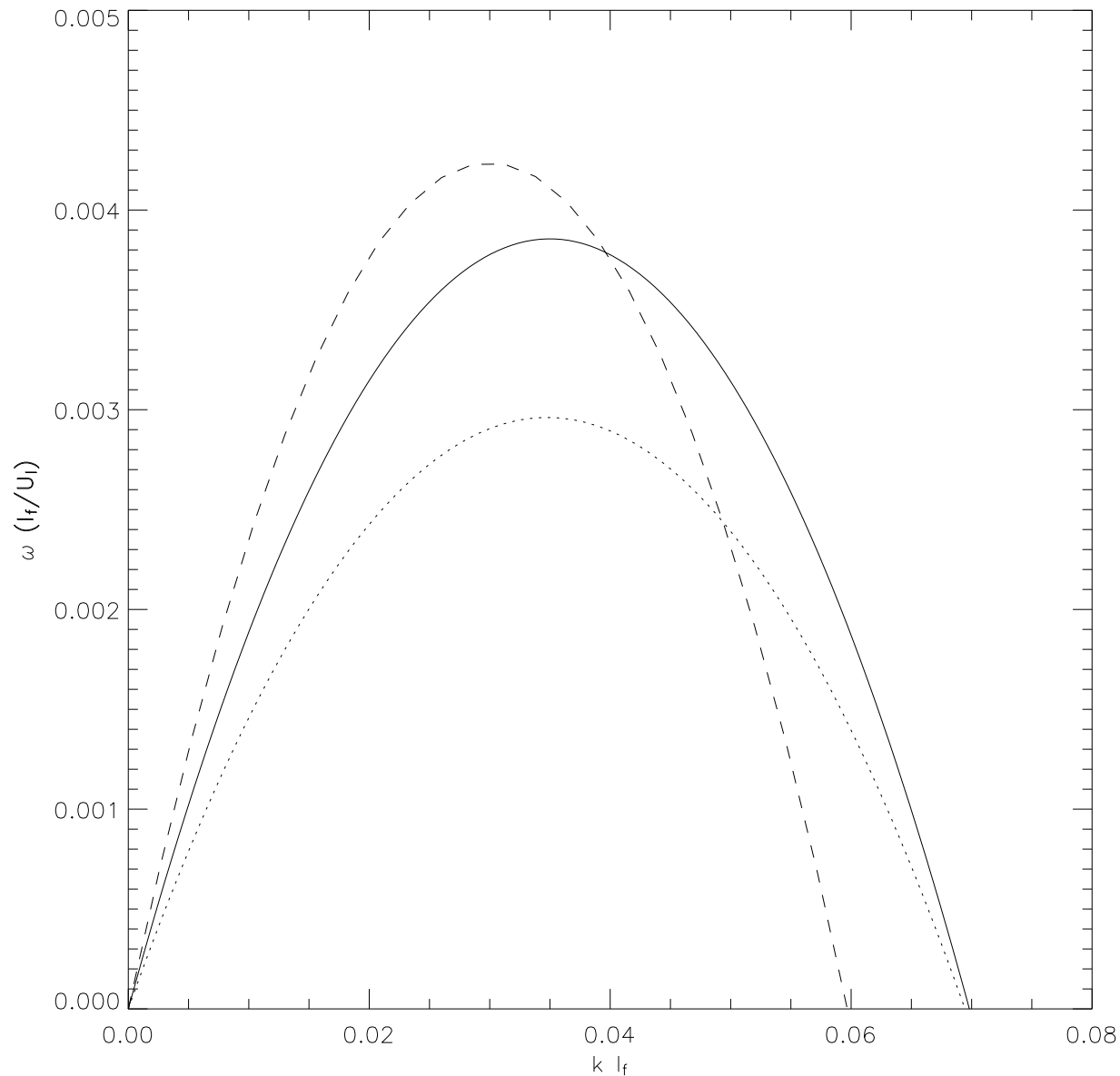


Fig. 8.— Predicted non-dimensional growth rate ($\omega l_f/U_l$) of the LD instability as a function of dimensionless wavenumber ($k l_f$) from Equation [1] for the three different densities, $2 \times 10^7 \text{ g cm}^{-3}$ (dashed), $4 \times 10^7 \text{ g cm}^{-3}$ (solid), and $8 \times 10^7 \text{ g cm}^{-3}$ (dotted), based on the measured Markstein numbers.

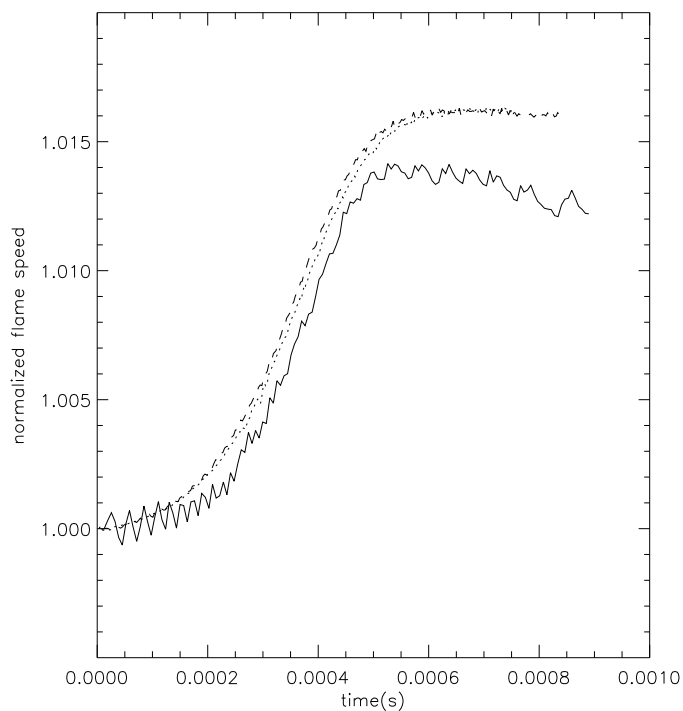


Fig. 9.— Normalized flame speed, $V_{\text{eff}}(t)/V_{\text{eff}}(t = 0)$, vs. time for the $4 \times 10^7 \text{ g cm}^{-3}$ LD unstable in a 10.24 cm wide domain at 3 different resolutions: 3.0 zones/ l_f (solid), 5.9 zones/ l_f (dash), and 11.8 zones/ l_f (dot). The two highest resolution runs seem to have converged. The main calculations presented in this paper were computed at the 5.9 zones/ l_f resolution. The normalization is required to correct for the small differences in the laminar flame speed with resolution.

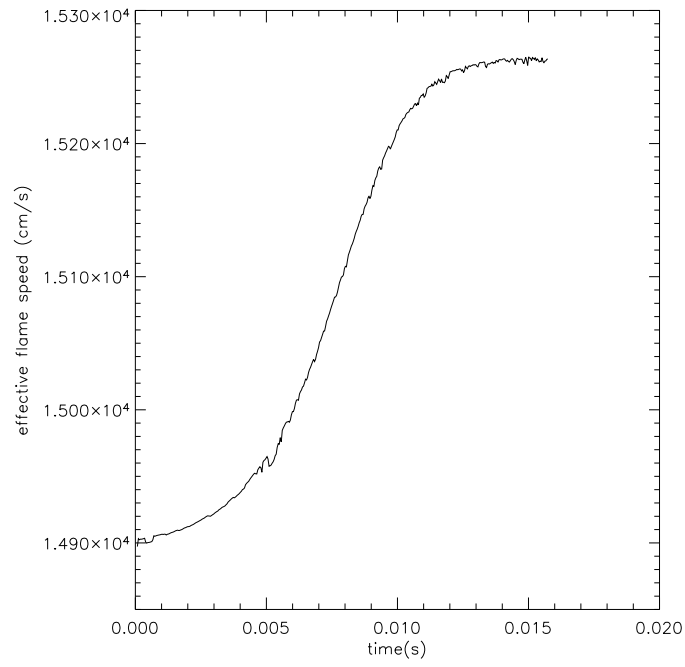


Fig. 10.— Flame speed as a function of time for the $2 \times 10^7 \text{ g cm}^{-3}$ LD unstable flame.

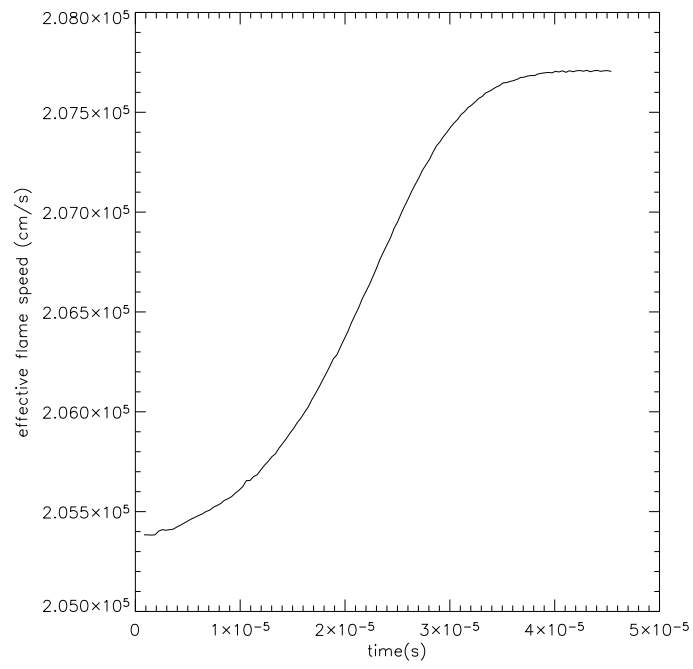


Fig. 11.— Flame speed as a function of time for the $8 \times 10^7 \text{ g cm}^{-3}$ LD unstable flame.

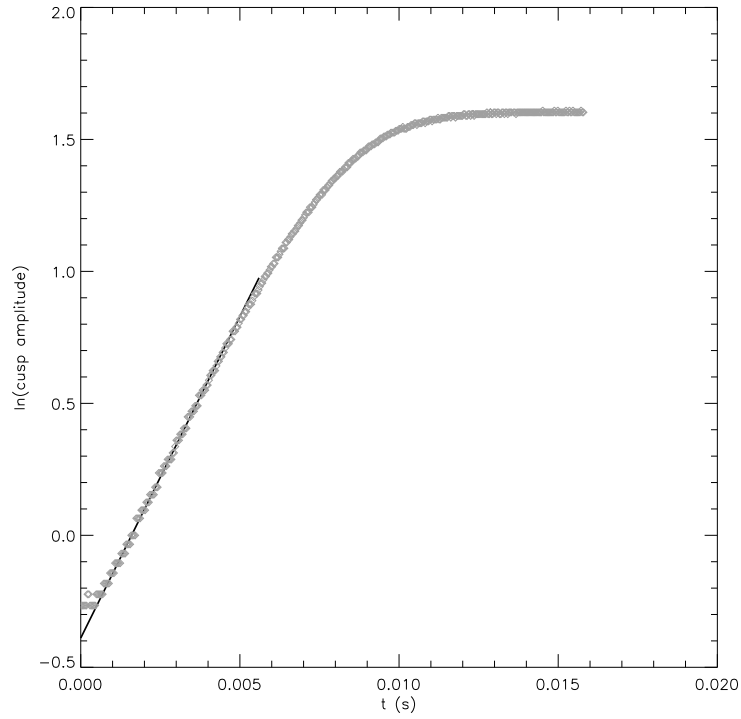


Fig. 12.— Cusp amplitude (natural log scale) as a function of time (symbols) and a fit on an exponential to the linear part (solid line) for the $2 \times 10^7 \text{ g cm}^{-3}$ flame, in the interval $[10^{-3} \text{ s}, 4 \times 10^{-3} \text{ s}]$. The growth rate of the fit is $\omega = 244 \text{ s}^{-1}$.

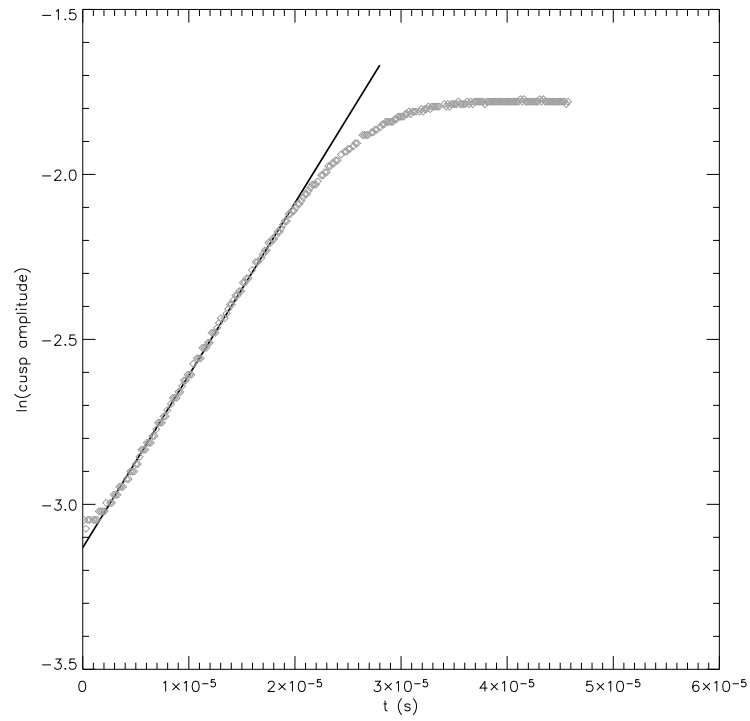


Fig. 13.— Cusp amplitude (natural log scale) as a function of time (symbols) and a fit on an exponential to the linear part (solid line) for the $8 \times 10^7 \text{ g cm}^{-3}$ flame, in the interval $[5 \times 10^{-6} \text{ s}, 2 \times 10^{-5} \text{ s}]$. The growth rate of the fit is $\omega = 522000 \text{ s}^{-1}$.

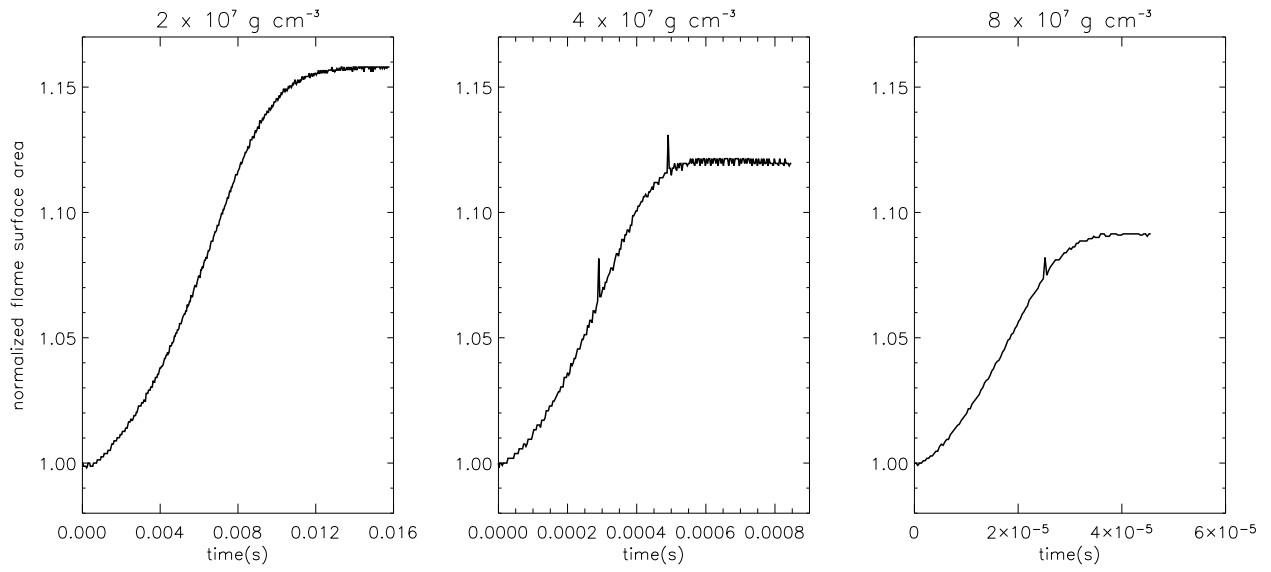


Fig. 14.— Normalized flame length, $L(t)/L(t = 0)$, as a function of time for the three different densities, $2 \times 10^7 \text{ g cm}^{-3}$ (left), $4 \times 10^7 \text{ g cm}^{-3}$ (center), and $8 \times 10^7 \text{ g cm}^{-3}$ (right). The increase in flame length is several times larger than the corresponding increase in the flame speed.